2018

High pressure phase transformations revisited

Valery I. Levitas
Iowa State University, vlevitas@iastate.edu

High pressure phase transformations revisited

Abstract
High pressure phase transformations play an important role in the search for new materials and material synthesis, as well as in geophysics. However, they are poorly characterized, and phase transformation pressure and pressure hysteresis vary drastically in experiments of different researchers, with different pressure transmitting media, and with different material suppliers. Here we review the current state, challenges in studying phase transformations under high pressure, and the possible ways in overcoming the challenges. This field is critically compared with fields of phase transformations under normal pressure in steels and shape memory alloys, as well as plastic deformation of materials. The main reason for the above mentioned discrepancy is the lack of understanding that there is a fundamental difference between pressure-induced transformations under hydrostatic conditions, stress-induced transformations under nonhydrostatic conditions below yield, and strain-induced transformations during plastic flow. Each of these types of transformations has different mechanisms and requires a completely different thermodynamic and kinetic description and experimental characterization. In comparison with other fields the following challenges are indicated for high pressure phase transformation: (a) initial and evolving microstructure is not included in characterization of transformations; (b) continuum theory is poorly developed; (c) heterogeneous stress and strain fields in experiments are not determined, which leads to confusing material transformational properties with a system behavior. Some ways to advance the field of high pressure phase transformations are suggested. The key points are: (a) to take into account plastic deformations and microstructure evolution during transformations; (b) to formulate phase transformation criteria and kinetic equations in terms of stress and plastic strain tensors (instead of pressure alone); (c) to develop multiscale continuum theories, and (d) to couple experimental, theoretical, and computational studies of the behavior of a tested sample to extract information about fields of stress and strain tensors and concentration of high pressure phase, transformation criteria and kinetics. The ideal characterization should contain complete information which is required for simulation of the same experiments.

Disciplines
Condensed Matter Physics | Geophysics and Seismology | Materials Science and Engineering | Structural Materials

Comments
This is a manuscript of the article Levitas, Valery. "High pressure phase transformations revisited." *Journal of Physics: Condensed Matter* (2018). DOI: 10.1088/1361-648X/aab4b0. Posted with permission.

Journal of Physics: Condensed Matter

High pressure phase transformations revisited

To cite this article before publication: Valery Levitas *et al* 2018 *J. Phys.: Condens. Matter* in press https://doi.org/10.1088/1361-648X/aab4b0

Viewpoint

High pressure phase transformations revisited

Valery I. Levitas
Iowa State University, Departments of Aerospace Engineering, Mechanical Engineering, and Material Science and Engineering, Ames, Iowa 50011, USA
Ames Laboratory,
Division of Materials Science and Engineering, Ames, IA, USA
Email: vlevitas@iastate.edu

Abstract

High pressure phase transformations play an important role in the search for new materials and material synthesis, as well as in geophysics. However, they are poorly characterized, and phase transformation pressure and pressure hysteresis vary drastically in experiments of different researchers, with different pressure transmitting media, and with different material suppliers. Here we review the current state, challenges in studying phase transformations under high pressure, and the possible ways in overcoming the challenges. This field is critically compared with fields of phase transformations under normal pressure in steels and shape memory alloys, as well as plastic deformation of materials. The main reason for the above mentioned discrepancy is the lack of understanding that there is a fundamental difference between pressure-induced transformations under hydrostatic conditions, stress-induced transformations under nonhydrostatic conditions below yield, and strain-induced transformations during plastic flow. Each of these types of transformations has different mechanisms and requires a completely different thermodynamic and kinetic description and experimental characterization. In comparison with other fields the following challenges are indicated for high pressure phase transformation: (a) initial and evolving microstructure is not included in characterization of transformations; (b) continuum theory is poorly developed; (c) heterogeneous stress and strain fields in experiments are not determined, which leads to confusing material transformational properties with a system behavior. Some ways to advance the field of high pressure phase transformations are suggested. The key points are: (a) to take into account plastic deformations and microstructure evolution during transformations; (b) to formulate phase transformation criteria and kinetic equations in terms of stress and plastic strain tensors (instead of pressure alone); (c) to develop multiscale continuum theories, and (d) to couple experimental, theoretical, and computational studies of the behavior of a tested sample to extract information about fields of stress and strain tensors and concentration of high pressure phase, transformation criteria and kinetics. The ideal characterization should contain complete information which is required for simulation of the same experiments.

1. Introduction

Under application of high pressure almost all materials transform to different phases changing their crystallographic structures. The high pressure phases have lower molecular volume; that is why high pressure is an effective tool to obtain them. High pressure phase transformations (PTs) are of great interest in the search for new high pressure phases with unique properties. Some of these phases became important materials for various engineering applications after their industrial synthesis had been established. For example, industrial synthesis of the diamond from graphite and superhard cubic boron nitride (BN) from graphite-like boron nitride occurs in the pressure range of 5-10 GPa and temperatures of 1500-2000 K. Also, high pressure PTs play a key role in geophysics and planetary science.

A major part of static high pressure research is performed in a diamond anvil cell (DAC), in which a sample is compressed between two diamonds up to a desired high pressure. To create

hydrostatic conditions the sample is placed in a liquid/gas or in materials with a low yield strength (quasi-hydrostatic media), which are sealed within a deformable gasket made of strong materials (stainless steel, tantalum, tungsten, rhenium, and even superhard cubic BN and diamond powders). The material's behavior is characterized in terms of the pressure p – specific volume v (per unit mass, mole, or atom) curve and phase transformations are detected by jumps in volume and changes in x-ray diffraction (XRD) patterns characterizing crystallographic structure, and/or by a change in the Raman spectra.

For each material the pressure-temperature phase diagram is developed, which contains regions of stability of various phases. Each phase boundary is defined theoretically from the conditions of equality of corresponding Gibbs energies. In experiments, significant deviation of the actual transformation start lines from the phase equilibrium lines is observed. Thus, PTs to high pressure phases occur at pressures higher than the equilibrium pressure, and reverse PT occurs below the phase equilibrium pressure or does not occur at all at a complete pressure release. This leads to metastable phases at normal pressure, which can be potentially used in engineering applications. This is one of the applied reasons why actual phase transformation kinetics under large deviation from the thermodynamic equilibrium should be studied. Such a deviation of PT pressure from the equilibrium one leads to complex hysteretic behavior under loading-unloading and regions of metastability of phases. For example, phase equilibrium pressure between graphite and diamond at room temperature is ~2 GPa. However, under hydrostatic conditions graphite transforms to diamond at 70 GPa (Ref. 1) and diamond never transforms back at zero pressure even under any large tensile stress, which only lead to its fracture. Thus, actual (rather than equilibrium) transformation diagrams are reported for various materials. However, they are not treated as fundamental properties of phase transformations but rather as a result of messy kinetics, which was almost never characterized experimentally and described theoretically in detail. Also, pressure for PT initiation is not a complete characteristic either, *e.g.*, PT from hexagonal to wurtzitic BN starts at 8.1 GPa but does not complete even at 25 GPa [2]. In addition, numerous metastable phases may appear under different conditions, which are not present in the equilibrium phase diagram at all but may be important for applications. Thus, silicon (and germanium) has just one stable high pressure phase, Si II, at a pressure below 20 GPa but almost a dozen metastable phases [3].

2. Effect of nonhydrostatic stresses

Though the PTs are called pressure-induced, in reality they occur in most cases under nonhydrostatic conditions. In these cases three principle stresses or generally six components σ_{ij} of the symmetric stress tensor $\boldsymbol{\sigma}$ act on material and material response is described by six components ε^{ij} of the strain tensor $\boldsymbol{\varepsilon}$, which (for simplicity, in geometrically linear approximation) usually includes elastic $\boldsymbol{\varepsilon}_t$, thermal $\boldsymbol{\varepsilon}_\theta$, transformational $\boldsymbol{\varepsilon}_t$, and plastic $\boldsymbol{\varepsilon}_p$ contributions, i.e., $\boldsymbol{\varepsilon} = \boldsymbol{\varepsilon}_e + \boldsymbol{\varepsilon}_\theta + \boldsymbol{\varepsilon}_t + \boldsymbol{\varepsilon}_p$. In addition, crystal lattice rotation occurs leading to texture formation or transformation of a single crystal into twinned or polycrystalline aggregate. Thus, information required for the description of material behavior is getting much more complicated than a single scalar relationship between pressure, volume, and temperature (i.e., equation of state). We will focus on experiments at constant temperature near room temperature or at least below recrystallization temperature, so that viscous relaxation of nonhydrostatic (called also deviatoric) stresses can be neglected. Transformation strain can be determined by mapping the crystal lattice of the single crystal of the low pressure phase into that of the high pressure phase for a stress-free case. Then all six components of the stress tensor affect the phase equilibrium and transformation conditions through expression for transformation work, $X_m = \boldsymbol{\sigma} : \boldsymbol{\varepsilon}_t = \sigma_{ij}\varepsilon_t^{ij}$, where summation over

repeated indices is assumed. Thus, the contribution of each component of the stress tensor to the thermodynamic driving force for transformation can be evaluated from this expression. An additional mechanical contribution is related to a jump of the elastic moduli during transformations and is in many cases less pronounced.

The effect of nonhydrostatic stresses on high pressure PTs has not been elucidated quantitatively in experiments. Major efforts are directed to reducing the degree of nonhydrostaticity by reducing the yield strength of the transmitting media. Such experiments are called under "quasi-hydrostatic" conditions, and since such conditions are not quantified, results strongly depend on transmitting media. E.g., by changing transmitting media from hydrostatic to highly nonhydrostatic, both the α→ε and reverse ε → α PT start pressure in iron can be changed in the range of 10-16 GPa [4]. The PT completion pressure range is reported in the range of 15.3 to 25.4 GPa for the α→ε PT and in the range of 3.7-8 GPa for the reverse ε → α PT [4]. These studies at least partially explain (but not quantify) even larger scatter in experimental data on PT in iron in literature (collected in Ref. 4-5), with "phase equilibrium" pressure in the range of 6-14 GPa, α→ε PT start and finish pressures in the range of 8.6-16 GPa and 14-25.4 GPa, respectively, and the reverse ε → α PT start and finish pressures in the range of 7-16.2 GPa and 1-8.5 GPa, respectively. As it will be discussed below the effect of nonhydrostatic stresses is quite limited, and it is plastic strain that is responsible for the above scatter.

3. Effect of plastic strain

3.1. Limited effect of the macroscopic nonhydrostatic stresses

Superposition of plastic shear on high pressure drastically reduces PT pressure [6-11], in some cases by an order of magnitude [8]. These results have been obtained in rotational Bridgman or rotational diamond anvil cells. Since PT pressure is in some cases getting smaller than the phase equilibrium pressure, the conclusion was made that plastic shear reduces phase equilibrium pressure as well [6]. Note that traditional continuum thermodynamics supplemented by the effect of deviatoric stresses cannot explain such a strong effect of shear stresses [12]. Indeed, the mechanical contribution to the thermodynamic driving force under action of pressure p and shear stress τ is: $X_m=-p\varepsilon_0+\tau\gamma$, where ε_0 and γ are the volumetric and shear transformation strains; the sign – is because the volumetric strain is negative and positive pressure p produces a positive contribution to the driving force for transformation. However, shear stress τ is limited by the yield strength in shear, say 1 GPa to make an order of magnitude estimate. Assuming for simplicity $\varepsilon_0=-\gamma$, we obtain $X_m=-(p+\tau)\varepsilon_0$. Thus, the same driving force X under hydrostatic conditions and under shear stress will be when pressure is reduced by the value of shear stress τ. If PT pressure under hydrostatic conditions is 10 GPa or 50 GPa, the shear stress can reduce these numbers to 9 and 49 GPa, respectively, i.e., by 10% and 2% only. Thus, applied shear stress cannot explain reduction in PT pressure by several times or an order of magnitude.

3.2. Classification of PTs

A resolution of these paradoxical results was suggested in [9-10]. First, *classification of high-pressure PTs* has been suggested. In most cases nucleation of the product phase occurs heterogeneously at some defects (dislocations, grain and twin boundaries), which produce a concentration of the stress tensor and/or provide some initial surface energy. *Temperature-induced* transformations nucleate predominantly at pre-existing defects without stresses at the specimen surface. Similarly, *pressure-induced* transformations occur mostly by nucleation at the same pre-existing defects under action of external hydrostatic pressure. *Stress-induced* transformations occur at the same defects when external nonhydrostatic stresses do not exceed the macroscopic yield strength in compression σ_y. If the PTs take place during plastic deformations they are classified as *strain-induced* transformations. They occur by nucleation at new defects generated during plastic

deformation. A similar classification (but without pressure-induced transformations and any relation to high pressure) was used for PTs in steels [13]. The main point in Refs. [9-10] was that the strain-induced PTs require completely different theoretical (thermodynamic) treatment and experimental characterization. The number of pre-existing nucleation sites (defects) is limited. That is why for pressure and stress-induced PTs one has to increase pressure or stresses to activate less potent defects (i.e., defects with a smaller stress concentrator, e.g., dislocation pile-ups with smaller number of dislocations). This explains the spreading of the PT over the broad pressure range. In contrast, plastic flow generates new defects and consequently new nucleation sites. First, this means that there are no needs to increase pressure; PT can be driven by increasing plastic shear and generating new defects at constant pressure, and new high pressure phase nuclei will appear near tips of these strong defects. Nuclei cannot grow significantly, because stresses decrease with distance away from the defect tip. However, the number of defects with nuclei at the tip of the new defects increases, filling the major part or entire sample. Second, stress concentration at the plastic strain-generated defects may be much stronger than for the preexisting defects. For example, the concentration of all components of the stress tensor at the tip of the dislocation pile up is proportional to the number of dislocations in a pile up, and it can be as large as 10 to 100. Thus, one needs much smaller external pressures to produce the same required PT pressure in a small region near the tip of a strong defect. This explains the significant reduction of the applied PT pressure in experiments. This mechanism has been confirmed more quantitatively utilizing an analytical model of nucleation at the dislocation pile up in Refs. [9-10] and phase field simulations of strain-induced PT in a bi-crystal in Ref. [12,14]. While we will not focus on strain-induced PT in rotational DAC here, the main point is that in major cases *PTs in traditional DAC and even in a perfectly hydrostatic medium include plastic straining and should be treated to some extent as strain-induced PTs* as well. Indeed, without a hydrostatic medium the pressure growth in DAC occurs during plastic compression of the sample or the sample within a gasket, since a final thickness of a sample after pressure release is essentially smaller than the initial thickness. The same is true for a solid-state "hydrostatic" medium, which still possesses finite yield strength and can impose shear stresses on a sample. As it was discussed in Refs. [9-10,15,16], there is *no fundamental difference* between strain-induced PTs under plastic compression in *traditional DAC and under pressure and shear in rotational DAC* in terms of mechanism, thermodynamics, and kinetics. The only difference is in the pressure-plastic strain path for each material point of the sample. In rotational DAC pressure can in principle be kept constant during torsion and PT (see, e.g., Ref. [17]), that is why it can be kept low and these experiments exhibit the strongest effect of plastic straining on PT pressure. In traditional DAC plastic straining occurs during increasing force and consequently pressure, even if is not required for PT[15]. Because of this, the promoting effect of plastic straining is hidden. Thus, the growth of pressure required to continue and complete PT in DAC is not a fundamental property of the PT thermodynamics and kinetics but the result of sample-loading system behavior.

As it was mentioned above, pressures for initiation and completion of direct and reverse PTs in experiments under nonhydrostatic conditions in DAC have drastic scatter in different papers and in the same paper for different transmitting media[4]. In most cases without transmitting media the reasons for discrepancy were not clear. However, if one would consider these *PTs as strain-induced rather than pressure-induced, the difference is caused by different plastic strain which was not measured nor even discussed*. Different geometric parameters and elastoplastic properties of the gasket, transmitting media, and sample lead to different plastic strains and, consequently, transformation pressure and pressure-concentration of high pressure phase curves. Thus, experimental results *do not characterize thermodynamic and kinetics of a sample material* but represent complex behavior of the sample-gasket (and, at very high pressure, anvil) system. Finite element modeling of PT in DAC as the strain-induced PTs[15,18,19] based on the theory developed in

Refs. [9-10,15] supported this statement. With the same mechanical properties, thermodynamic and kinetic parameters of a sample, different ratios of the yield strength of the gasket and sample σ_g/σ_{y1} and different radii and heights of a sample led to different pressures for initiation and completion of PT and the entire pressure - concentration of high pressure phase, c, curves (Fig. 1). These system parameters change degree, direction, and heterogeneity of plastic flow and sliding (friction) at the contact surfaces between sample, diamonds, and gasket, causing change in strain-controlled PT kinetics.

Consequently, *plastic strain is a primary parameter*, which should be measured or calculated along with pressure and concentration of high-pressure phase.

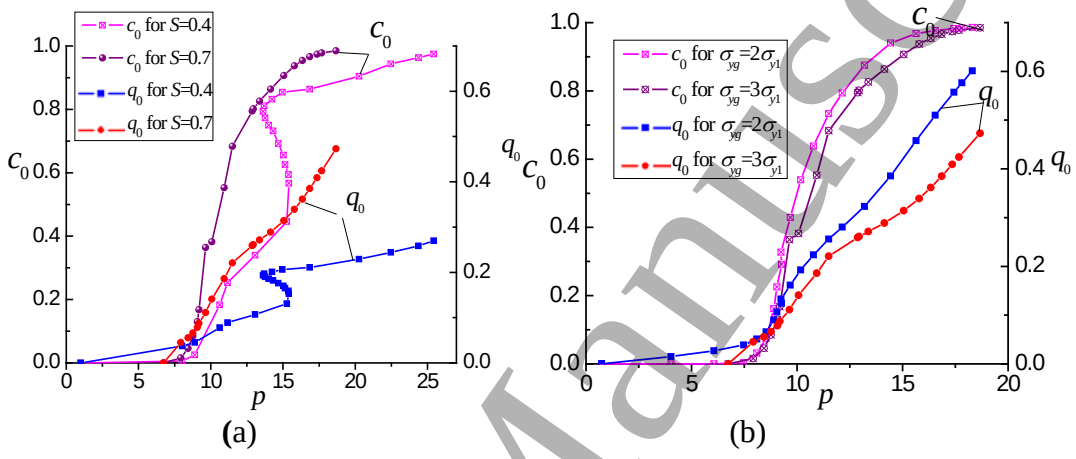

Fig. 1. Variations of concentration of high-pressure phase c_0 and accumulated plastic strain q_0 averaged over the deformed sample thickness at the symmetry axis versus pressure p at the contact surface at the symmetry axis. (a) for $\sigma_{yg}=3\sigma_{y1}$ and different relative radii of a sample over the radius of the cullet $S=0.4$ and $S=0.7$; (b) For S=0.7 and with different gasket strengths $\sigma_{yg}=3\sigma_{y1}$ and $\sigma_{yg}=2\sigma_{y1}$. Adopted from [18].

3.3. Characterization of phase transformations at high pressure

The question arises: *what would be the ideal experimental characterization of phase transformations in high pressure experiments?* During elastoplastic compression of a sample and gasket, with or without phase transformations, all fields are extremely heterogeneous and not all of them can be measured or have been measured. To extract information from experiments these heterogeneous fields should be modeled. This leads us to the following definition:

Ideal characterization should contain complete information which is required for simulating the same experiments.

Then, by quantitative comparison and fitting experimental and simulated fields, one can extract information about material behavior, and complete material characterization and models at some level of complexity and accuracy. Without continuum theory it is impossible to do. Thus, characterization involves development of continuum theories for the description of processes in diamond anvils, which includes coupled kinetic equations for elastoplastic deformations and phase transformations, which can be solved in the sample and surrounding components (gasket and anvils).

4. Relationship between theory and experiment and simulation of technological processes

Let us compare the relationship between theory and experiment and technological applications for several disciplines.

High pressure science is experimentally driven. We are not discussing atomistic simulations here, which lead to predictions of new phases and determination of material properties under pressure, see Ref. [20-22] as examples. Our point is that there is no continuum theory describing transformation kinetics, hysteresis (metastability), the effect of the stress tensor and plastic strain, except some works described above[15-19,23-26]. However, those models were not calibrated by experiment. That is why there is no simulation tool for high pressure technologies. The only exception is modeling efforts on industrial diamond synthesis which, however, were also not fully fitted to experiments[27,28]. The effect of the stress tensor in that case was not important because graphite transforms to diamond inside of liquid metal. The probable reason for the lack of continuum theory is the existence of numerous new phases and exciting phenomena[20-22,29-33] to be discovered, and desire to achieve maximum pressure and measure all physical parameters that could be measured. This seems to be much more attractive and topically closer for physicists, material scientists, chemists, and geophysicists than worrying about heterogeneities of parameters and focusing on continuum theories. It should be mentioned that continuum theories required for the description of processes in diamond anvils are extremely complex. They include: (a) physical nonlinearities (nonlinear elasticity, plasticity, phase transformations); (b) geometric nonlinearities (large elastic, plastic, and transformational strains and lattice rotations); and (c) contact nonlinearities (sliding and cohesion along the contact surfaces between different materials, variable contact zone, and combination of the Coulomb and plastic friction), and their coupling. Also, both phase transformation and plasticity are multiscale phenomena and models at different scales are quite different.

Let us consider the current trends in some other disciplines.

Plasticity. There are numerous text books on plasticity[34-36] and corresponding courses. Most parts of the books consist of theory and sophisticated equations. Equations are formulated for a 3D case and arbitrary complex stress and plastic strain tensor histories. There is a limited number of experiments to calibrate and verify models, usually under homogeneous 1D and 2D stress-strain states. In the first approximation, material behavior is described by an experimentally determined stress-strain (or plastic strain) curve in tension, compression, or torsion. With the help of the simplest von Mises plasticity theory with isotropic hardening this curve completely determines plastic deformation under complex 3D loading. While these and much more sophisticated phenomenological models have never been directly checked under complex 3D loading they are broadly and successfully applied to simulate and optimize technological processes, like forging, extrusion, sheet forming, and so on. This means that even with existing inaccuracies these models have predictive power and applied significance. Definitely, even a simple model is much better than no model at all, which should be accepted by the high pressure community.

Phase transformations in shape memory alloys. For martensitic PTs austenite transforms to a finite number of crystallographically equivalent martensitic variants. Theories of different complexities describe PTs in terms of the concentration of martensite[37], or concentrations of martensitic variants (e.g., 3 variants for cubic to tetragonal transformation)[38,39], or (at larger scale) concentrations of habit plane variants (e.g., 24 habit plane variants for cubic to tetragonal transformation, each consisting of a fine mixture of two martensitic variants)[40-44]. Thus, in addition to an austenite-martensite transformation, variant-variant transformations, which represent in most cases twinning, are described. Since volumetric transformation strain for phase transformations in shape memory alloys is almost zero, the effect of hydrostatic pressure is negligible and phase

transformations are solely driven by the deviatoric stress tensor. Similar to plasticity, 3D constitutive equations are formulated under a general stress tensor. Kinetic equations for the rate of concentration of each variant are formulated in terms of the thermodynamic driving forces conjugate to the rate of corresponding concentration. They include both temperature and effect of deviatoric stress tensor. The effect of plasticity in most cases is neglected. Similar to plasticity theory there is a limited number of experiments to calibrate and verify models, usually under homogeneous 1D and 2D stress-strain states. These models are applied to simulate behavior of structures made of shape memory alloys[37,45], including actuators, energy absorbers, medical devices, and components assembly based on shape memory effects.

Phase transformations in steels are classified as temperature-induced (with no external stresses), stress-induced (for external stresses below the yield strength), and strain-induced when PT occurs during plastic deformation[13,46-48]. Each type of transformation is modeled in a different way but internal stresses and elastic and plastic strains are important for all of them. Thermally-induced PTs are broadly modeled for heat treatment of steels and for material design. Stress-induced transformations are mostly modeled in order to describe transformation-induced plasticity (TRIP) [49], which occurs due to internal stresses caused by heterogeneous transformation strain under external stresses below the yield strength. Strain-induced transformations in steel are usually described based on a martensite nucleation model at the intersection of shear bands[46,47,50,51]. It is also formulated for a 3D case for concentration of product phase and transformation strain versus stress tensor and plastic strain tensor history and calibrated and verified by a limited number of experiments[49,50,52-54]. Models are applied to simulate technological processes, like thermal and thermomechanical treatment, see e.g. Ref. [54].

Note that in all of these fields there are continuum models at different scales and different complexities. For example, in plasticity there are models based on discrete dislocations (traditional and phase field models), dislocation densities, single crystal plasticity, polycrystalline aggregates, and macroscopic phenomenological flow theories. Similarly, for phase transformations there are models based on detailed resolution of microstructure (sharp interfaces and phase field modeling), crystallographic and micromechanical models of martensite in a single and polycrystals, and phenomenological macroscopic models. There are sophisticated methods to measure stress and displacement fields and attempted to connect them for calibration and verification of micromechanical models, e.g., in Ref. [55-57].

Thus, in plasticity and PTs in steels and shape memory alloy, continuum theories are quite well developed and play an important part in extraction of material properties from experiments. It should be our goal to do the same for high pressure science. The best initial point is to start with the simplest macroscale models, similar to the von Mises theory in plasticity.

5. Directions for coupled measurements, modeling, simulations, and characterization of different types of phase transformations under high pressure

5.1. Pressure-induced transformations

Let us consider a spherical particle placed in the ideal liquid under high pressure, i.e., under ideal hydrostatic conditions[58-61]. Let the spherical nucleus or macroscopic region of high pressure phase appear at the center of initial sphere, keeping spherical symmetry. Due to jump in a specific volume (or transformation volumetric strain) during PT, the nucleus of the high pressure phase will pull the remaining part of the hollow sphere of the low pressure phase. As a result, while the internal sphere remains under hydrostatic conditions, the pressure in it significantly reduces. The hollow sphere of low pressure phase is under nonhydrostatic conditions, and when (for the jump in volume exceeding a few percents) the magnitude of the difference between radial and hoop stress exceeds the yield

strength, plastic flow in the low pressure phase near the phase interface will take place. In the course of PT plastic strain and dislocation and/or twin structure in the low pressure are inherited by the high pressure phase. In this region the stress state is becoming nonhydrostatic and additional plastic deformation in the high pressure phase may occur. Thus, even in the most ideal situation phase transitions in solids occur in most cases under local nonhydrostatic conditions and in the presence of plastic deformation. This has been known for a long time[62] for hydrostatic loading of a polycrystalline sample, in which internal stresses result in broadening of diffraction lines. Also, cyclic direct-reverse PTs under increasing-decreasing pressure is accompanied by an increase in hardness, transformation pressure for direct PT, and pressure hysteresis[6]. This is the so-called transformation hardening phenomenon, which also occurs for temperature-induced cyclic PTs. It is connected to plastic deformation caused by internal stresses due to heterogeneous transformation strain evolution during PTs. Under hydrostatic conditions the shape of the polycrystalline sample does not change, so this plasticity is not measurable at the scale of the sample.

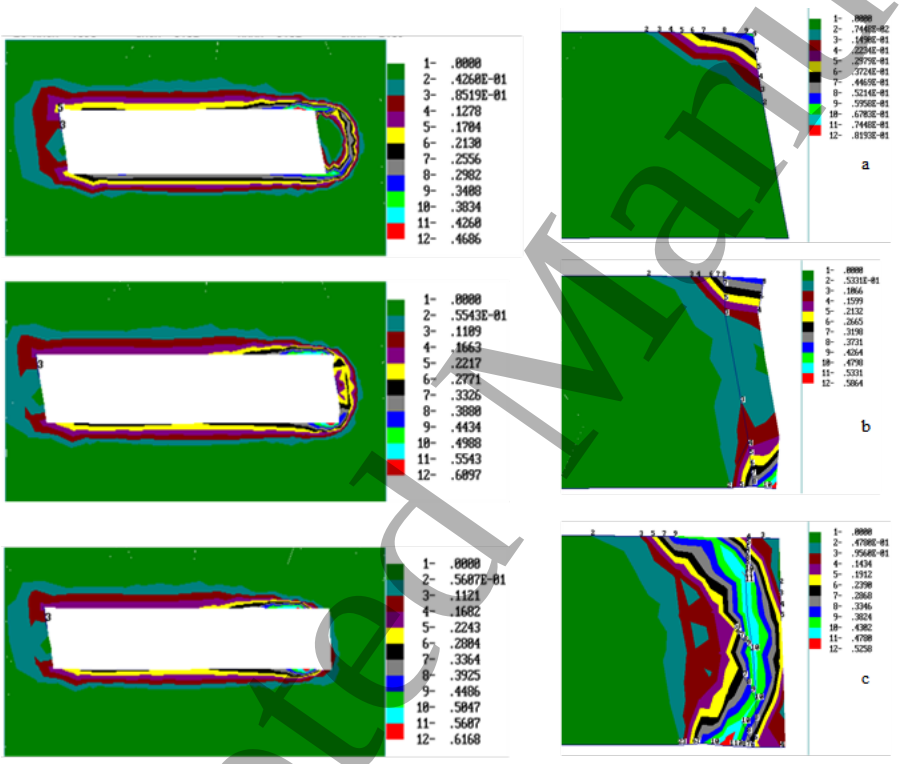

Fig. 2. Isobands of the accumulated plastic strain q in austenite around growing martensitic plate (white region in the left figure) and in the right part of the martensitic plate (right figure). Adopted from [63].

Even without pressure, just for temperature-induced martensitic PT in steel, large plastic strain is accumulated during PT, see Fig. 2 from Ref. [63]. Despite the relatively small transformation volumetric strain ε_{0t}=0.02 and shear of 0.2, the accumulated plastic strain q (defined from $\dot{q} = (2/3\mathbf{d}_p : \mathbf{d}_p)^{1/2}$, where $\mathbf{d}_p$ is the plastic deformation rate; for uniaxial compression or tension, q is reduced to the logarithmic strain) within the martensitic plate and surrounding austenite is around 0.6! Plastic strain first appears in a weaker austenite, then it is inherited by the growing

martensitic plate which causes huge internal stresses and additional plastic deformations in both. It is shown in Ref. [63] that the plastic strain arrests martensitic plate growth and is responsible for the plate to lath morphological transition.

Deviation of the actual transformation pressure p from the phase equilibrium pressure p_e is caused by the following reasons:

(a) Nucleation barrier.
(b) Energy of internal stresses.
(c) Athermal interface friction (dissipation) caused by Peierls barrier, interaction of a moving interface with stress field of various defects, e.g. point defects (solute and impurity atoms, vacancies), dislocations, grain, subgrain and twin boundaries and precipitates.

Phase transformation progress in elastoplastic material is determined by the thermodynamic PT criterion[59-60,64-66]

$$X=K, \qquad (1)$$

where X is the thermodynamic driving force for PT and K is the athermal threshold. The general expression for X in Ref. [59-60,64-66] is quite sophisticated and requires knowledge of plastic strain and internal stress evolution during each transformation increment. Also, X depends on the geometry of the evolving microstructure. For phase transformation in elastic materials X is equal to the difference between the Gibbs energy of the initial and final states, and the actual geometry and the internal structure of the transformed regions (when interface dissipation is neglected) is determined by the principle of minimum of the Gibbs energy, or $X \rightarrow max$. When plastic and interface dissipations are included the principle of minimum of the Gibbs energy is not applicable. With the help of the postulate of realizability the following extremum principle, $X\text{-}K \rightarrow max$, for each transformation increment is justified in [59,64-66]. Examples of application of this approach for the description of temperature- and stress-induced PTs can be found in Refs. [9,51,59-60,64-66] and in the application to pressure-induced PT in a DAC, in Refs. [24,25]. However, to extract experimental information and develop simplified models of pressure-induced PTs, which can be used for simulation of a *pressure-induced* PT, one can transform PT criterion $X=K$ to a simplified expression for transformation pressure

$$p_t = p_e + b(c)\sigma_y(c,q) \pm a(c)\sigma_y(c,q) \quad \text{or} \quad p_t = p_e + b_H(c)H(c,q) \pm a_H(c)H(c,q), \qquad (2)$$

where the signs ± is for direct and reverse PTs, c is the concentration of the high pressure phase; a, b and a_H , b_H are factors to be determined from experiment, and σ_y and H are the yield strength and hardness of the two-phase mixture of low- and high-pressure phases. Eq.(2) can be obtained from Eq.(1) by specifying the expression for X and K and dividing by volumetric transformation strain ε_{0t} . Since the yield strength and hardness are proportional to each other, both Eqs.(2) are equivalent. The first term on the top of the phase equilibrium pressure p_e is the back pressure due to energy of internal stresses caused by volumetric transformation strain ε_0, which is the same for direct and reverse PTs and, consequently, does not contribute to the pressure hysteresis. Proportionality of the back pressure to the yield strength is accepted because the contributions to X due to internal stresses, when they cause plastic flow, are proportional to σ_y [58-61]. The last term in Eq.(2) is K/ε_{0t}. There are several hints that make Eq.(2) a good starting point for the description of pressure-induced PTs. In Ref. [6], pressure hysteresis (i.e., difference between initiation pressure for the direct and reverse PT) for a number of materials (RbCl, KCl, KBr, CdS, CdSe, Ce, InSb, Bi) for different degrees of

preliminary plastic deformation, was found to be proportional to the hardness of the low pressure phase after deformation. According to Eq.(2), pressure hysteresis (defined as the difference in the pressure for initiation of the direct PT and pressure for initiation of the reverse PT after completing the direct PT) is

$$h = a(0)\sigma_y(0,q) + a(1)\sigma_y(1,q+\Delta q) = \sigma_y(0,q)[a(0) + a(1)\sigma_y(1,q+\Delta q)/\sigma_y(0,q)],$$

where Δq is the increment of plastic strain after complete direct PT. If the term in square parenthesis is weakly dependent on plastic strain *q*, then $h \sim \sigma_y(0,q)$, in correspondence with experimental data in Ref. [6]. Independently, one of the often used assumptions is that the phase equilibrium pressure is a semisum of the pressure of initiation of the direct and reverse PTs. In this case,

$$a(0)\sigma_y(0,q) = a(1)\sigma_y(1,q+\Delta q) \text{ and } h = 2a(0)\sigma_y(0,q) \sim \sigma_y(0,q).$$

Based on the above experiments and some analytical solutions it was suggested in Ref. [59,64] that the athermal threshold *K* is proportional to $\sigma_y(q)$. This seems reasonable because the threshold *K* characterizes an interaction between a moving interface and the material's microstructure and the yield strength characterizes the resistance to the motion of dislocations through the same microstructure (obstacles). Proportionality between *K* and $\sigma_y(q)$ is also proved for temperature-induced martensitic PT in steels[67] and utilized in simulations in Ref. [63].

Eq.(2) explains in a simple way the main reason for the significant scatter in PT pressure vs. concentration (or just for initiation and completing of PTs). Pressure-concentration curve depends on the yield strength and plastic strain, which were not characterized. Initial samples could be produced by different methods (rolling, extrusion, or others) and have different values of the yield strength, which characterizes microstructure. Depending on the value of strain, the yield strength may change by a factor of 1.5 to 5 for different materials[34]. At large strains (*q>0.4* for rocks and *q>1* for metals), according to the regularity revealed in Ref. [34], σ_y, *H*, and, consequently, *K* are becoming strain and strain-history independent. In this case transformation pressure is a function of *c* only. Thus, two steps could be made in order to achieve consistent characterization of pressure-induced PTs under external hydrostatic pressure:

(a) Perform pressure-induced characterization after large plastic deformation of a sample and achieve maximum yield strength (hardness),
(b) Perform pressure-induced characterization after annealing and different degrees of preliminary plastic deformation of a sample and measuring hardness (or yield strength).

This would be the first quantitative characterization and description of pressure-induced PTs, which has accuracy comparable to the accuracy of the phenomenological flow theory plasticity [36] and theory for thermally-induced PTs [67].

We cannot a priori exclude that even in the maximum hardened state there is a possibility that $p_t(c)$ curves for direct and reverse transformation may depend on the mode of preliminary plastic deformation (compression, shear, or any their combinations). Before reaching the maximum hardened state the chances that the mode of preliminary plastic straining makes a difference are higher. Also, texture and internal stresses due to possibly heterogeneous preliminary plastic deformation may play an important role and lead to scatter in the $p_t(c)$ or $p_t(c,q)$ relationship.

In the next approximations a more sophisticated micromechanically-based theory can be developed, like those in plasticity and PT in shape memory alloys. They are based on the

consideration of a polycrystalline sample consisting of multiple single crystals and the consideration of transformation strain tensors for each crystallographically equivalent variant. This could be simplified analytical models or detailed finite element or spectral method modeling of each of the single crystal within polycrystalline sample. Such simulations can be compared with much more detailed experiments [68-81], in which elastic strain tensor in each individual grain is measured, and orientation of each individual grain. Currently, such measurements are mostly utilized for studying plasticity under high pressure, but there are first works on studying PTs [70,80,82].

5.2. Stress-induced phase transformations under high pressure

In the first approximation, Eq. (2) can be generalized in the following form

$$-\left(p_t - b(c)\sigma_y(c,q)\right)\varepsilon_{0t} + \left(\boldsymbol{S} - A(c)\sigma_y(c,q)\boldsymbol{e}_t\right)\boldsymbol{:}\,\boldsymbol{e}_t = -p_e\ \varepsilon_{0t} \mp a(c)\sigma_y(c,q)\varepsilon_{0t} \quad (3)$$

or

$$p_t = p_e + b(c)\sigma_y(c,q)\ \pm a(c)\sigma_y(c,q) + \left(\boldsymbol{S} - A(c)\sigma_y(c,q)\boldsymbol{e}_t\right)\boldsymbol{:}\,\boldsymbol{e}_t / \varepsilon_{0t}, \quad (4)$$

where $\boldsymbol{S}:\boldsymbol{e}_t = S_{ij}e_{ij}^t$ is the work of deviatoric stress tensor $\boldsymbol{S} = \{S_{ij}\}$ along the deviatoric transformation strain tensor $\boldsymbol{e}_t = \{e_{ij}^t\}$, and $A(c)\sigma_y(c,q)\boldsymbol{e}_t$ is the deviatoric back stress due to internal stresses, which is similar to the back pressure assumed to be proportional to $\sigma_y(c,q)$. While for simplicity we assume proportionality of the deviatoric back stress to $\boldsymbol{e}_t$, more complex evolution equations are possible, similar to the plasticity [34-36] theory and shape memory alloys [40-45]. We also assumed for simplicity that the direction $\boldsymbol{n} = \boldsymbol{S}/|\boldsymbol{S}|$ of the stress deviator in the stress space does not change during PT. Without work of the deviatoric stresses Eq.(3) is equivalent to Eq.(2). The left-hand side of Eq. (3) is the transformation work of stresses minus back stresses. The contribution due to deviatoric stresses and transformation strain in Eq. (4) is always positive for

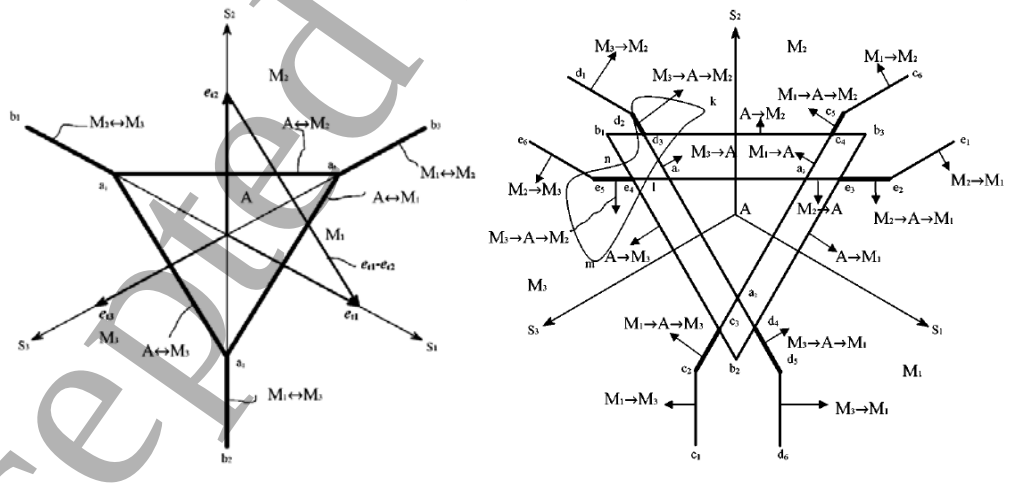

Fig. 3. Phase equilibrium (left) and transformation (right) lines in the deviatoric stress S_i plane . S_i axes are projections of σ_i axes into deviatoric plane. Deviatoric transformation strain vectors $\boldsymbol{e}_{ti}$ for each of the crystallographically equivalent variants M_i are directed along the S_i axes. Cubic-tetragonal equilibrium lines are orthogonal to vectors e_{ti} and form a triangle. Within the triangle austenitic cubic phase A is stable, outside of it the tetragonal martensitic variants M_i are stable. The boundary between variants $M_i - M_j$ is orthogonal to $\boldsymbol{e}_{ti} - \boldsymbol{e}_{tj}$ and coincides with S_k. Transformation lines are obtained by splitting each of equilibrium lines into two parallel lines, which leads to complex hysteretic behavior. Reproduced from [83].

direct PT and often positive for the reverse PT. Since ε_{0t} is negative for pressure-induced PTs, deviatoric stresses reduce transformation pressure for the direct PT and often for the reverse PTs. Geometrically, conditions of phase equilibrium and transformations for a single crystal can be presented in the six-dimensional space of the components of the stress tensor, similar to the yield surface in plasticity theory. For example, for cubic to tetragonal PT, which has 3 crystallographically equivalent variants, these conditions can be presented in the three-dimensional space of normal stresses σ_i orthogonal to the cubic (and tetragonal) faces. For each fixed pressure, phase equilibrium and transformations conditions can be presented in the deviatoric stress S_i plane (see Fig. 3), which is equally inclined to all three axes σ_i and orthogonal to the hydrostatic line $\sigma_1 = \sigma_2 = \sigma_3$. Transformation strains for any variant can be determined based on lattice parameters of low and high pressure phases. For all other variants the components of the transformation strain can be easily obtained by symmetry operations. Thus, to use Eq. (4), one should measure deviatoric stresses in addition to the measurements for pressure-induced PT. Recently [84-85], molecular dynamics simulations for cubic to tetragonal PT Si I↔Si II have determined the PT conditions in 3D stress space of stresses σ_i normal to the cubic phases (Fig. 4). In agreement with the prediction of the phase field approach [86], PT conditions are linear in σ_i and independent of shear stresses.

Eq.(4) can also be applied for each specific variant,

$$p_t = p_e + b(c_i)\sigma_y(c_i,q) \pm a(c_i)\sigma_y(c_i,q) + (\boldsymbol{S} - A(c_i)\sigma_y(c_i,q)\boldsymbol{e}_{ti}) : \boldsymbol{e}_{ti} / \varepsilon_{0t}, \qquad (5)$$

where $\boldsymbol{e}_{ti}$ and c_i is the transformation strain and concentration for i^{th} variant. Since all variants are equivalent, functions a and σ_y should be the same for any variant and in the first approximation should depend on the total concentration $c = c_1 + c_2 + c_3 + \ldots$. The total deviatoric transformation strain is determined by the mixture rule $\boldsymbol{e}_t = c_1\boldsymbol{e}_{t1} + c_2\boldsymbol{e}_{t2} + c_3\boldsymbol{e}_{t3} + \ldots$. This is a more detailed description than in terms of the total concentration of the high pressure phase. Also, there is no need to assume for such a description that the direction $\boldsymbol{n} = \boldsymbol{S}/|\boldsymbol{S}|$ is unchanged during PT.

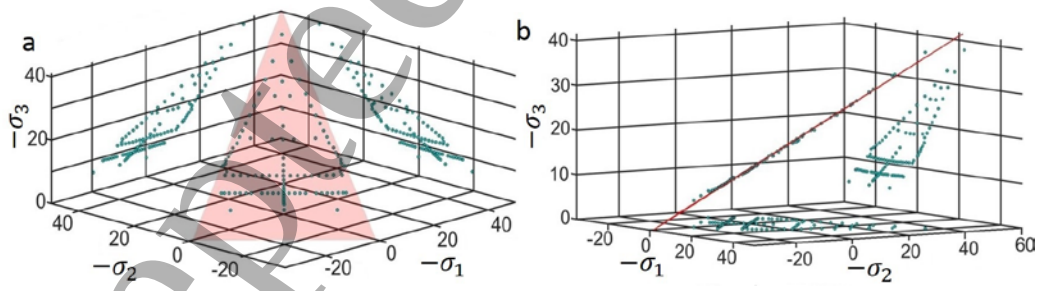

Fig. 4. Confirmation of the phase transformation (lattice instability) criterion obtained with the phase field approach in [86] for Si I→Si II PT. (A) Plane in stress space σ_i corresponding to the PT criterion and corresponding instability points from the molecular dynamics simulations. (B) The same plot as in (A) but rotated until theoretical plane is visible as a line, to demonstrate how close the simulation points and the theoretical plane are. Adopted from [85].

For a polycrystalline sample or when each c_i cannot be determined, $\boldsymbol{e}_t$ depends on deviatoric stress $\boldsymbol{S}$. For micromechanical models of single and polycrystals it can be assumed or derived that for the unchanged direction $\boldsymbol{n}$ one has

$$\boldsymbol{e}_t = \lambda \boldsymbol{S}\,, \qquad (6)$$

where λ is a scalar, which is determined either theoretically or experimentally [37,49]. Scalar λ may depend on concentration *c* and also on the stress mode, because in some cases the magnitude of the transformation strain is different for tension, compression and torsion [52-53]. With the help of Eq. (6), Eq.(4) transforms to

$$p_t = p_e + b(c)\sigma_y(c,q) \pm a(c)\sigma_y(c,q) + \lambda \boldsymbol{S}:\boldsymbol{S}\left(1-\lambda A(c)\sigma_y(c,q)\right)/\varepsilon_{0t}\,, \qquad (7)$$

where $\boldsymbol{S}:\boldsymbol{S} = 2/3\sigma_i > 0$, $\sigma_i > 0$ is the equivalent von Mises stress, which is often used in plasticity theory (in particular, $\sigma_i = \sigma_y$ for von Mises plasticity condition). Eq.(7) corresponds to two coaxial circles in the deviatoric stress plane. Since for direct PT $\lambda > 0$, $\lambda A(c)\sigma_y(c,q) < 1$ (magnitude of stress is greater than the magnitude of the back stress), and $\varepsilon_{0t} < 0$, it is clear that deviatoric stresses reduce PT pressure. If the second and third terms in Eq.(5) are the same as for loading under hydrostatic conditions, then all parameters (excluding λ) can be determined in hydrostatic experiment and then used for nonhydrostatic conditions. Parameter $\lambda(c)$ can be found from one experiment with specific $p(c)$ and $\boldsymbol{S}(c)$ measured experimentally and substituted in Eq.(6). Then Eqs.(6) and (7) can be used for any other loading conditions. To measure $\boldsymbol{e}_t$ directly, one has to measure change of shape of a sample under pressure which will be discussed in Section 5.3.

The key difference between characterization of PTs under hydrostatic and nonhydrostatic conditions is that under nonhydrostatic conditions the stress-strain state is usually quite heterogeneous in the sample. Thus, nonhomogeneous fields should be measured, calculated, and fitted to each other in order to extract all parameters in the constitutive equations and characterize a PT. The main problem here is that usually high pressure is produced in the course of plastic compression of the sample and gasket. Even with transmitting media, if it supports the nonhydrostatic stresses it may produce plastic strain in a sample as well. Even when external deviatoric stresses are much below the yield strength the total (external and internal) stresses can meet the yield criterion, and cause TRIP.

Thus, it is very difficult to produce stress-induced PTs and to separate them from the strain-induced PTs in high pressure experiments. Because of this we will focus on more widespread strain-induced PTs.

5.3. Strain-induced phase transformations under high pressure

In this case the contribution to the driving force for PT due to defects (stress concentrations) generated during plastic flow, which serve as nucleation sites, should be taken into account. This was done in Refs. [9-10] in terms of a coarse-grained microscale model based on barrierless nucleation on defects (e.g., dislocation pileups) generated during plastic flow and resulted in a strain-controlled kinetic equation:

$$\frac{dc}{dq} = k\frac{(1-c)\,\overline{p}_d H(\overline{p}_d)\dfrac{\sigma_{y2}}{\sigma_{y1}} - c\overline{p}_r H(\overline{p}_r)}{c + (1-c)\sigma_{y2}/\sigma_{y1}}; \qquad \overline{p}_d = \frac{p - p_\varepsilon^d}{p_h^d - p_\varepsilon^d}; \qquad \overline{p}_r = \frac{p - p_\varepsilon^r}{p_h^r - p_\varepsilon^r}. \qquad (8)$$

Here p_{ε}^{d} is the minimum pressure below which direct strain-induced PT to high pressure phase does not take place; p_{ε}^{r} is the maximum pressure above which reverse strain-induced PT to low pressure phase cannot occur; $\overline{p}_{d}$ and $\overline{p}_{r}$ are dimensionless characteristic pressures, which are used for direct and reverse PTs; p_{h}^{d} and p_{h}^{r} are the pressures at which direct and reverse PTs occur under hydrostatic loading, respectively; they may be a function of *c* and *q* (see Eq. (2)); σ_{y1} and σ_{y2} are the yield strength of the low and high pressure phases; *k* is a scaling parameter, and *H* is the Heaviside step function. There are more general versions of Eq. (8) [9-10]. However, it also operates with pressure and volumetric transformation strain only and should be generalized for the full stress and transformation strain tensors.

Note that (a) nucleation is barrierless and does not require thermal fluctuations, and (b) stress concentration near the tip of the defect sharply reduces away from the defect, the nucleus reaches thermodynamic equilibrium and does not grow further. Thus, time is not a parameter and accumulated plastic strain *q* is a time-like parameter. Since defects generate stresses of opposite signs in the different regions they promote both direct and reverse PTs. That is why Eq.(8) takes into account contributions due to both direct and reverse PTs. Also, in a two-phase mixture plastic strain is localized in the phase with the smaller yield strength; this is the reason for the appearance of the ratio of the yield strengths of phases in Eq. (8).

Eq. (8) combined with macroscopic equations for coupled large elastoplastic deformations and PTs has been utilized in analytical [9-10] and finite element studies of strain-induced PTs in ordinary [15,18,19,87,88] and rotational DAC [16,23,26]. Various experimental phenomena have been reproduced and interpreted. However, material parameters in Eq.(8) were not determined for any material, because of a lack of corresponding experimental data. Usually, the pressure distribution along the contact surface between sample and diamond is measured [6,11,17,89-95], which in combination with a measurement of the sample thickness under the load allows one to determine the pressure dependence of the yield strength in shear [34,91,93,95] and distribution of the shear stresses at the contact surface. The elastic strain tensor was measured in some selected spots of a sample using axial or radial XRD [70,72,74,82,90,96-103]. When elastic single crystal moduli at high pressure were known and with the help of an assumption connecting single and polycrystalline elastic properties, the differential stress was determined, i.e., the difference between axial and radial principle stress. If plastic flow occurs, then this stress is equal to the yield strength in compression under a given pressure. Alternatively, deviatoric stress is evaluated utilizing width of x-ray peaks [104,105]. However, we are not aware of publications that present experimentally-determined deviatoric stress *distribution* in DAC. Concentration of high pressure phase averaged along the thickness of a sample has been measured for several distances from the center of a sample in Ref. [17]. In principle there are currently methods that allow one to measure the distribution of elastic lattice strain that may be converted into distribution of stresses [70,72,74]. However, the main problem is that a *distribution* of *plastic strain was not directly measured*. That is why it was impossible to extract information for calibrating kinetic Eq. (8). Note that the recent development[106] of high-resolution transmission X-ray microscopy has enabled 3D tomography and measurement of the shape and volume of the sample loaded in a liquid transmitting medium in DAC with 30-nm spatial resolution. Such a technique has been used for studying the deformation of metallic glasses under hydrostatic pressure.[107,108] This opens perspectives to measuring the total strain tensor of an entire sample or particles embedded in a sample and, after accounting for the elastic strain tensor, determining plastic strain. Distribution of the displacement of ruby particles placed at the contact surface between the anvil and the sample was measured in Ref. [109,110]. For measurement of the thickness of the sample under load, the method based on the electric capacity sensor can be used.[111]

The method of x-ray laminography was utilized for reconstruction of a sample geometry in DAC[112] and measurement of the displacement distribution of the Pt strain marker representing the plane passing through the symmetry axes of a sample in rotational DAC.[113]

Information about the distribution of displacements obtained by the aforementioned methods, along with measured pressure distribution, can be utilized for comparison with FEM simulations. However, the problem is that the friction conditions at the contact surface are not well-defined and they may affect both simulations and experiments. This problem should be studied separately. Alternatively, one can place metallic non-transforming particles with known elastic properties under high pressure and use XRD to measure both elastic strain and positions (displacements) of particles. An advantage of x-ray measurements is that these particles can be placed in some middle plane of a sample by dividing a cylindrical sample into two cylinders of smaller height and placing these parts one above another. Double information could be obtained if displacements of both particles at the sample-diamond boundary and inside of the sample will be determined simultaneously or consecutively. One of the possibilities is to place metallic particles at the symmetry plane of a sample and focus an x-ray beam at this plane, both on particles and sample material without particles. Shear stresses and strains at the symmetry plane are zero, so only principle stresses and strains are present which simplifies the processing of experimental data and comparison with computations. Also, since the x-ray spot will average measurements from both sides of the symmetry plane, this will be equivalent to the reduction of the spot size by a factor of two from the point of view of the heterogeneity of fields along the thickness. This is especially important for very high pressures and a thin sample. Another possibility is to place metallic particles very close to the sample-diamond boundary. This (along with displacements of the ruby particles at the sample-diamond boundary) will allow one to determine the total strain distribution in a thin contact layer of a sample. The stress state in this layer is a superposition of hydrostatic (mean) pressure (i.e., all normal stress components are equal) and maximum shear stress, which is similar to the stress state at the sample-diamond boundary in rotational DAC. A comparison of transformation behavior at two different stress modes (states) is important due to the following reasons. First, stress mode may affect the PT kinetics, which is the case for some TRIP steels [50,52-53]. This should be included in Eq.(6) and quantified. Second, if the effect of stress mode is negligible, this significantly simplifies the theory and experimental determination of transformation kinetics.

Results of simulations, even with model material parameters, give hints about possible approaches to extract strain-controlled PT kinetics from the experiment. Thus, if the high pressure phase is significantly weaker than the low pressure phase, it is currently almost impossible to extract strain-controlled PT kinetics from the experiment, because PT leads to strain-softening and multiple instabilities in the form of shear and transformation bands [15,16,18,19,23,26]. During plastic compression of materials without a gasket and with a large pressure gradient there are some steps at pressure distribution with almost constant pressure, which are usually located at the boundary between low and high pressure phases. It was found in simulations that for materials with stronger high pressure phases these steps correspond to pressure between p_ε^d and p_ε^r values [15,16,18,19,23], which allows one to determine these parameters in the first approximation. Also, pressure at some steps is the same for compression and torsion for fullerene [11], which confirms the idea that there is no basic difference in strain-induced kinetics for processes in DAC and rotational DAC. At the same time, similar steps for a weaker high pressure phase do not have any specific importance for determining PT kinetics [15,16,18,19,23].

One of the most important results in Ref. [18] consists of the suggested method to extract full kinetic information (including plastic strain) from experiments for a stronger high-pressure phase for a sample within a gasket. Since all calculated fields (including plastic strain) are quite homogeneous at the center of the sample (Fig. 5), stresses and concentration of the high pressure phase can be

easily measured and plastic strain can be calculated based on changes in sample thickness under the load.

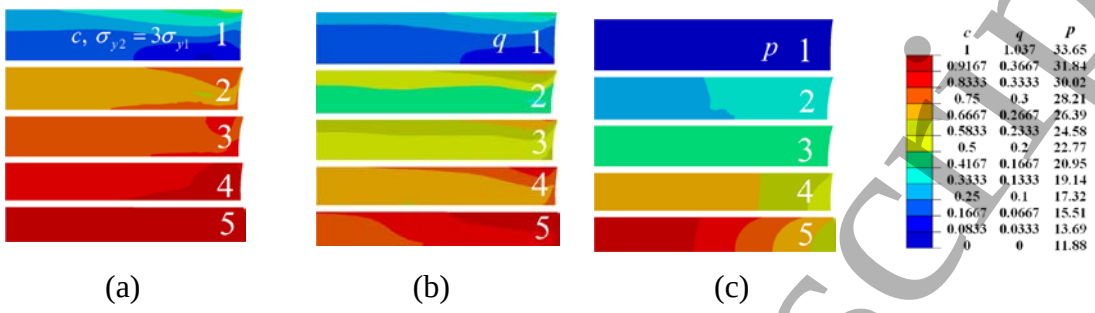

(a) (b) (c)

Fig. 5. Distributions of (a) concentration of high-pressure phase *c*, (b) accumulated plastic strain *q*, and (c) dimensionless pressure *p*, in the half of a sample within a gasket (not shown) for increasing applied force. All parameters are distributed relatively homogeneously at the center of the sample. Reproduced from Ref. [18].

In general, to simplify the determination of kinetic information, it is desirable to preliminarily heavily deform the sample plastically at normal pressure to reach a state of maximum hardening. Then the effect of plastic strain on the yield strength of the phases will be excluded, which significantly simplifies both model and comparison with experiments. As a first step one can determine pressure dependence of the yield strength for pure low pressure and high pressure phases by compressing the sample without or with a gasket with significant reduction in thickness, measuring the pressure gradient and sample thickness, and comparing results with simulations [34,91,93,95]. With known elastic properties of phases, the distribution of all components of the stress tensor can be calculated and compared with distributions obtained by an XRD measurement of elastic strain [34,70,72,74,82,96-103]. Making these two distributions consistent is not a trivial task, the solution of which would eliminate or at least minimize indeterminacies in Refs. [34,70,72,74,82,96-103].

A comparison of measured and calculated displacement fields will allow one to verify or improve the model of plastic flow at high pressure. Actually, finite element modeling of plastic flow in DAC offers quite good correspondence with experiments [90] in terms of pressure distribution and shape of the sample-anvil boundary up to 300 GPa, see Ref. [114,115]. Then focus should be on PTs with a measuring field of concentration of high pressure phases by relative intensities of X-ray peaks. The best way to characterize coupled PTs and plastic flow is to use the sample with a strong gasket that produces conditions of a quasi-homogeneous state in the central part of the sample [17,18]. This will allow one to determine the pressure and concentration dependence of the yield strength of the mixture of low and high pressure phases and strain-controlled kinetics. If one can plastically deform a two phase mixture without PT (e.g., by reducing pressure and then reloading and plastically deforming below p_ε^d), then plastic properties can be decoupled from the transformation. Then, considering a coupled PT and plastic flow and evaluating plastic strain based on the measurement of the reduction of sample thickness, one can determine extra plastic strain due to PT. This is so called TRIP, which can be very large in experiments when external stresses satisfy the plasticity condition, as it was shown in Ref [17]. By varying ratios of height to diameter of a sample and radius of a sample to radius of an anvil, gasket material, and pressure-plastic strain trajectory at each point (which can be varied significantly [18]) one can obtain a broad spectrum of kinetic data for comparison between experiments and simulations.

After experiments under quasi-homogeneous conditions and characterizing kinetics and plasticity, one can repeat the same combined experiments and simulations for conditions with large pressure gradients and check equations for larger plastic strain and pressure. Some caution, however, should be exercised in the interpretation of experiments. During torsion the thickness of a sample reduces and the high-pressure phase radially flows to the low-pressure region. If it does not transform back, one may have made a wrong conclusion that high pressure phase appeared at pressure significantly lower than in reality [15,16]. Both experimental and computational results should be connected to material rather than to spatial points (Lagrangian description), at least by recalculations.

Note that q represents a geometric rather than a physical characteristic of plastic strain. It would be much more convenient and physically sound to substitute it with a physically based measure of plastic strain, which can be measured in situ, e.g., by XRD. As an example, it was found in Ref. [17] for hexagonal BN that the concentration of turbostratic stacking fault, which was measured in situ based on relative broadening of some diffraction peaks, is proportional to the plastic strain, i.e., is a physical measure of plastic strain for layered structures. This, in particular, allowed revealing TRIP, which is proportional to change in concentration of the high pressure phase, and separate TRIP from conventional plasticity, which is proportional to the angle of rotation of an anvil. For metals a similar parameter may be a dislocation density. However, at very large strain these parameters may saturate (similar to saturation of strain hardening).

5.4. Some experimental methods

Modern methods allow the study of plastic flow and PTs in detail in micrometer-scale volumes [68,69,73] utilizing synchrotron radiation. These methods have been further developed for studying material compressed in DAC using axial or radial XRD [70-72,82,90]. Thus, in Ref. [70] combined plastic flow and PTs between α, γ, and ε phases in polycrystalline iron have been studied under a special pressure-temperature program. Changes in pressure, differential stress, concentration of phases, and texture have been recorded. Some models and codes describing texture formation due to PT [74] and plasticity [116] are utilized to select the most plausible mechanisms describing observed texture.

Three-dimensional X-ray diffraction (3D-XRD) can be used for characterizing the orientation, position, and elastic strain tensor of single grains in a polycrystalline aggregate [68-69,71-73,98] and dislocation density [71]. Grain position, however, is not well defined in Ref. [72]. 3D-XRD has not been used for studying PTs yet. However, plastic strain is not measured in these experiments, which prevents the determination of kinetic equations. The possibility of utilizing dislocation densities along different slip systems, which was measured in Ref. [71], instead of plastic strain should be explored. Also, heterogeneity of stress and strain distributions within DAC was neglected. To extract kinetic information from these experiments, a more sophisticated micromechanically-based theory should be developed, like those in plasticity and PT in shape memory alloys. They are based on considering a polycrystalline sample consisting of multiple single crystals and considering transformation strain tensors for each crystallographically equivalent variant. This could be simplified using analytical models, self-consistent approaches [108], or detailed finite element or spectral method modeling of each of the single crystals within a polycrystalline sample. However, natural logics of development of each discipline first requires developing the simplest macroscopic models with minimum governing and material parameters, and their calibration with the simplest experiments. This will allow one to determine a distribution of all fields within a sample compressed in DAC. Then for selected small volumes with known macroscale strain and stress tensors history, one can perform more detailed coupled simulations and

3D-XRD studies to calibrate models and study processes at the microscale. In such a way, a multiscale characterization and description can be performed.

Note that an increase in accuracy may completely change basic concepts and way of description. For example, in plasticity theory the engineering yield strength was determined as corresponding to the offset of plastic strain of 0.2%. With such an offset, experimental yield surfaces and their evolution have been determined in 2D stress space, e.g., for tension (compression) and torsion or tension and internal pressure for a tubular sample. There was a hope that reducing the offset of plastic strain significantly by increasing the accuracy of displacement measurement will allow for a more precise evolution of the yield surface during loading. However, with increasing accuracy microplasticity which occurs at local stress concentrators (like grain boundaries and triple junctions, dislocation pile-ups, and others) became measurable. It appeared that microplastic deformation starts at almost zero external stresses and occurs during unloading which compromised the idea of the yield surface. In this case, multiple internal variables describing the microheterogeneous plastic deformation have been introduced, utilizing rheological models or a micromechanical description. Similarly for PT, depending on the accepted offset on the concentration of the high pressure phase, which corresponds to the beginning of PT, different levels of complexity of characterization and description will be required.

6. Concluding remarks

Several important points for the study and characterization of high pressure PTs are made in this paper.

1. It is underlined that there are three different types of high pressure PTs, namely, *pressure-induced, stress-induced, and strain-induced* transformations. Each of these types of PTs requires completely different thermodynamic and kinetic treatments and experimental characterization. In most high pressure literature the difference between these types of PTs is neglected, which is one of the reasons for large scatter in the reported PT pressure. The key point is the interaction between PT and defect (e.g., dislocation) structure, which evolves during the transformation and deformation and which was neglected in high pressure science. Even under hydrostatic external pressure a change in volume and shape during the transformation causes nonhydrostatic stresses and plastic deformation.

2. Usually, plastic-strain induced PTs are studied under compression and torsion in rotational Bridgman anvils or rotational DAC. The main point is that since in major cases pressure growth in traditional DAC occurs during plastic compression of a sample or sample within a gasket, *PTs in DAC include plastic straining and should be treated as strain-induced PTs* as well. There is *no fundamental difference* between strain-induced PTs under plastic compression in *traditional DAC and under pressure and shear in rotational DAC* in terms of mechanism, thermodynamics, and kinetics. The only difference is in the pressure-plastic strain path for each material point of the sample.

3. During elastoplastic compression of a sample and gasket, all fields (stress and plastic strain tensors, concentration of high pressure phase, and others) are extremely heterogeneous and not all of them can be measured. To extract information from experiments these heterogeneous fields should be modeled and compared to experimentally determined fields. In particular, the finite element simulation of the plastic flow without PT in DAC [106,107] offers sufficient correspondence with experiments [90] up to 300 GPa.

4. This leads us to the following definition: *ideal characterization of high pressure PTs should contain complete information, which is required for simulation of the same experiments.*

5. A comparison of the relationship between theory, experiment, and simulation of technological applications for high pressure science, plasticity, stress-induced PTs in shape memory

alloys, and strain-induced PTs in steels is performed. In all these fields but high pressure science, theoretical continuum description and numerical simulation of heterogeneous fields play a leading role. All equations are formulated for the general 3D case and arbitrary complex stress and plastic strain tensor histories. Models of different degrees of complexity are formulated, calibrated and verified, usually under homogeneous 1D and 2D stress-strain states. While these and much more sophisticated phenomenological models have never been checked under complex 3D loading, they are broadly and successfully applied to simulate and optimize corresponding technological processes.

6. In contrast, high pressure science is experimentally driven. Even for the simplest pressure-induced PTs, there is no continuum theory describing transformation kinetics and hysteresis (metastability). For stress- and strain-induced PTs, there are some hypothetical models, which are not calibrated by experiment because of lack of coupled experimental and simulation efforts.

7. For pressure-induced PTs, deviation of actual transformation pressure from the phase equilibrium for each concentration of high pressure phase c is formalized to be proportional to the yield strength (or hardness) of material as a function of plastic strain and concentration c. This seems reasonable because the athermal threshold for interface motion K characterizes an interaction between a moving interface and the material's microstructure and the yield strength characterizes the motion of dislocations through the same obstacles. Thus, the missing parameter, which promises to eliminate big scatter in pressure for initiation and completing PT and entire PT kinetics, is the accumulated plastic strain and it can be characterized by hardness. If the correlation between plastic strain and width of the x-ray peak is found, then the entire characterization of pressure-induced PTs can be performed in situ.

8. For stress-induced PTs, two types of characterizations are suggested which both require measurement of deviatoric stresses. For a single crystal, and when it is possible to measure concentration of each crystallographic variant, the contribution of deviatoric stresses to the PT criterion and kinetic equation is completely determined by the measured constant transformation strain of each variant. When the description is in terms of the total concentration of the high pressure phase, then proportionality of deviatoric transformation strain and stresses is utilized and the proportionality factor should be determined from an experiment. A geometric interpretation of phase equilibrium and transformation conditions in the deviatoric stress plane is suggested. However, there is a problem with distinguishing stress-induced PTs and strain-induced PTs, which should be characterized in a completely different way.

9. Strain-induced PTs should be characterized in terms of strain-controlled kinetics. One of the nano- and micromechanically based kinetic equations is suggested for this purpose. It is currently used in finite element simulations but was not calibrated and directly verified against experiments. New experiments in traditional DAC and coupled experimental and computational procedures are suggested for calibrating this model. Some of them are based on a quasi-homogeneous stress-strain-concentration state in the middle of a sample within a gasket as predicted by simulations. Others are based on strongly heterogeneous states with a maximum pressure gradient, when shear stress at the sample-diamond surface reaches the yield strength in shear. The main problem is to find a way to determine plastic strain field.

10. After these simplest models are calibrated, verified, and used for characterization of all three types of PTs, much more sophisticated multiscale models and corresponding existing experimental techniques can be coupled to develop characterization of PTs at several smaller scales and with more detail.

Thus, recent progress in the classification of high pressure PTs, three-scale continuum theory and simulations, as well as progress in multiscale in-situ characterization of high pressure PTs and defect structure, open the way to qualitatively advance this field to the level similar to that in the PTs under normal pressure and plastic deformation of materials. The key point is in synergistic coupling of the modeling and experiments on PTs, plasticity, and microstructure evolution at several scales. Obtained information will lead to developing the nonequilibrium thermodynamics and kinetics in 6D space of the components of the stress tensor for stress-induced transformations and 12D space for strain-induced transformations (with additional six components of plastic strain tensor) instead of pressure. Additional dimensions will substitute scatter in transformation pressure with a quantitative description. Higher dimension space of governing parameters will lead to a computational design of pathways to synthesis of new phases and significant reduction in transformation pressure, as well as ways to retain high pressure phases at normal pressure.

Acknowledgements. The support of NSF (CMMI-1536925 and DMR-1434613), ARO (W911NF-17-1-0225), and Iowa State University (Vance Coffman Faculty Chair Professorship) are gratefully acknowledged. Discussions with and some suggestions from Drs. Russell Hemley and Maddury Somayazulu are very much appreciated.

References

1. Schindler T and Vohra Y 1995 *Journal of Physics: Condensed Matter* **7** L637
2. Solozhenko V L, Will G and Elf F 1996 *International Assoication for the Advancement of High pressure Science and Technology (AIRAPT); High Pressure Science and Technology - International Conference* (World Scientific Publishing)
3. Domnich V, Ge D B and Gogotsi Y 2004 *High Pressure Surface Science and Engineering. Section 3*, eds Gogotsi Y and Domnich V (Bristol: Institute of Physics) pp 381–442
4. Bargen N V and Boehler R 1990 *High Press. Res.* **6** 133
5. Zarkevich N A and Johnson D D 2015 *Phys. Rev. B* **91** 174104
6. Blank V D and Estrin E I 2014 *Phase Transitions in Solids under High Pressure* (New York: CRC Press)
7. Bridgman P W 1935 *Phys. Rev.* **48** 825-847
8. Ji C, Levitas V I, Zhu H, Chaudhuri J, Marathe A and Ma Y 2012 *Proc. Natl. Acad. Sci. of the USA* **109** 19108
9. Levitas V I 2004 *High Pressure Surface Science and Engineering. Section 3*, eds Gogotsi Y and Domnich V (Bristol: Institute of Physics) pp 195–292
10. Levitas V I 2004 *Phys. Rev. B* **70** 184118
11. Novikov N V, Polotnyak S B, Shvedov L K and Levitas V I 1999 *J. Superhard Mater.* **3** 39
12. Levitas V I and Javanbakht M 2014 *Nanoscale* **6** 162-166
13. Olson G B and Cohen M 1986 *Dislocations in Solids* vol 7, ed F R N Nabarro (Amsterdam: Elsevier science) pp 297–407
14. Javanbakht M and Levitas V I 2016 *Physical Review B* **94** 214104
15. Levitas V I and Zarechnyy O M 2010 *Phys. Rev. B* **82** 174123
16. Levitas V I and Zarechnyy O M 2010 *Phys. Rev. B* **82** 174124
17. Levitas V I, Ma Y Z, Hashemi J H, M and Guven N 2006 *J. Chem. Phys.* **125** 044507
18. Feng B, Levitas V I and Ma Y 2014 *J. Appl. Phys.* **115** 163509
19. Feng B, Levitas V I and Zarechnyy O M 2013 *J. Appl. Phys.* **114** 043506
20. Zhang W W, Oganov A R, Goncharov A F, Zhu Q, Boulfelfel S E, Lyakhov A O, Stavrou E, Somayazulu M, Prakapenka V B and Konopkova Z 2013 *Science* **342** 1502-1505
21. McMahan A K and Lesar R 1985 *Phys. Rev. Lett.* **54** 1929-1932
22. Zhu Q, Oganov A and Zhou X F 2014 *Topics Current Chem.* **345** 223-256
23. Feng B and Levitas V I 2013 *J. Appl. Phys.* **114** 213514
24. Polotnyak S B 2008 *J. Superhard Mater.* **30** 82
25. Polotnyak S B 2008 *J. Superhard Mater.* **30** 163
26. Feng B and Levitas V I 2016 *J. Appl. Physics* **19** 015902
27. Leshchuk A A, Novikov N V and Levitas V I 2001 *Strength Mater.* **33** 277-292
28. Novikov N V, Levitas V I, Leshchuk A A and Idesman A V 1991 *High Press. Res.* **7** 195-197
29. Struzhkin V 2016 *Science* **351** 1260-1262
30. Drozdov A P, Eremets M I, Troyan I A, Ksenofontov V and Shylin S I 2015 *Nature* **525** 73-76
31. Troyan I, Gavriliuk A, Rueffer R, Chumakov A, Mironovich A, Lyubutin I, Perekalin D, Drozdov A and Eremets M I 2016 *Science* **351** 1303-1306
32. Dubrovinsky L, Dubrovinskaia N and Bykova E *et al*. 2015 *Nature* **525** 226-229
33. Dias R P and Silvera I F 2017 *Science* **355** 715-718
34. Levitas V I 1996 *Large Deformation of Materials with Complex Rheological Properties at Normal and High Pressure* (New York: Nova Science)
35. Lubarda V A 2001 *Elastoplasticity Theory* (Boca Raton: CRC Press)
36. Lubliner J L 1990 *Plasticity Theory* (New York: Macmillan)

37. Levitas V I, Idesman A V and Stein E 1999 *Int. J. Intell. Mater. Syst. Struct.* **10** 983-996
38. Idesman A V, Levitas V I, Preston D L and Cho J Y 2005 *J. Mech. Phys. Solids* **53** 495-523
39. Roytburd A L 1998 *J. Appl. Phys.* **83** 228-238
40. Boyd J G and Lagoudas D C 1996 *Int. J. Plast.* **12** 805-842
41. Gao X J, Huang M S and Brinson L C 2000 *Int. J. Plast.* **16** 1345-1369
42. Lagoudas D C, Entchev P B, Popov P, Patoor E, Brinson L C and Gao X 2006 *Mechan. Mater.* **38** 430-462
43. Siredey N, Patoor E, Berveiller M and Eberhardt A 1999 *Int. J. Solids Struct.* **36** 4289-4315
44. Thamburaja P and Anand L 2001 *J. Mech. Phys. Solids* **49** 709-737
45. Brinson L C and Lammering R 1993 *Int. J. Solids Struct.* **30** 3261-3280
46. Olson G B 1984 *Deformation, Processing, and Structure*, ed G Krauss (Warrendale: ASM International) pp 391–424
47. Olson G B and Cohen M 1972 *J. Less-Common Metals* **28** 107
48. Olson G B and Cohen M 1975 *Metall. Trans. A* **6** 791
49. Fischer F D, Reisner G, Werner E, Tanaka K, Cailletaud G and Antretter T 2000 *Int. J. Plast.* **16** 723-748
50. Diani J M and Parks D M 1998 *J. Mech. Phys. Solids* **46** 1613-1635
51. Levitas V I, Idesman A V and Olson G B 1998 *Acta Mater.* **47** 219-233
52. Hecker S S, Stout M G, Staudhammer K P and Smith J L 1982 *Metall. Trans. A* **13** 619-626
53. Lebedev A A and Kosarchuk V V 2000 *Int. J. Plast.* **16** 749-767
54. Sitko M and Skoczen B 2012 *Int. J. Solids Struct.* **49** 613-634
55. Rollett A D, Rohrer G S and Suter R M 2015 *MRS Bulletin* **40** 951-958
56. Pokharel R, Lind J, Kanjarla A K, Lebensohn R A, Li S F, Kenesei P, Suter R M and Rollett A D 2014 *Annual Review of Condensed Matter Physics* **5** 317-346
57. Stebner A P, Vogel S C, Noebe R D, Sisneros T A, Clausen B, Brown D W, Garg A and Brinson L C 2013 *Journal of the Mechanics and Physics of Solids* **61** 2302-2330
58. Kaganova I M and Roitburd A L 1987 *Sov. Phys. Solid State* **29** 800-803
59. Levitas V I 1997 *J. Mech. Phys. Solids* **45** 923 -947
60. Levitas V I 1997 *J. Mech. Phys. Solids* **45** 1203 -1222
61. Roitburd A L and Temkin D E 1986 *Sov. Phys. Solid State* **28** 432-436
62. Weidner D J, Wang Y and Vaughan M T 1994 *Science* **266** 419
63. Levitas V I, Idesman A V, Olson G B and Stein E 2002 *Philos. Mag. A* **82** 429-462
64. Levitas V I 1998 *Int. J. Solids Struct.* **35** 889 -940
65. Levitas V I 2000 *Int. J. Plast.* **16** 805-849
66. Levitas V I 2000 *Int. J. Plast.* **16** 851-892
67. Ghosh G and Olson G B 1994 *Acta. Metall. Mater.* **42** 3361-3371
68. Ice G E and Larson B C 2000 *Adv. Eng. Mater.* **2** 643-646
69. Jensen D J, Lauridsen E, Margulies L, Poulsen H and Schmidt S 2006 *Mater. Today* **9** 18-25
70. Merkel S, Liermann H P, Miyagi L and Wenk H R 2013 *Acta Mater.* **61** 5144-5151
71. Nisr C, Ribarik G, Ungar T, Vaughan G B M, Cordier P and Merkel S 2012 *J. Geophys. Res.* **117** B03201
72. Nisr C, Ribarik G, Ungar T, Vaughan G B M and Merkel S 2014 *High Press. Res.* **34** 158-166
73. Poulsen H F 2004 *Tracts in Modern Physics* vol 205 (Berlin: Springer)
74. Wenk H R, Huensche I and Kestens L 2007 *Metal. Mater. Trans. A* **38** 261
75. Merkel S, Kubo A, Miyagi L, Speziale S, Duffy T S, Mao H K and Wenk H R 2006 *Science* **311** 644-646

76. Merkel S 2010 *High-Pressure Crystallography: From Fundamental Phenomena To Technological Applications*, eds E Boldyreva and P Dera (Dordrecht, The Netherlands: Springer Science) pp 111–122
77. Kanitpanyacharoen W, Merkel S, Miyagi L, Kaercher P, Tome C N, Wang Y, and Wenk H R 2012 *Acta Mater.* **60** 430-442
78. Liermann H P, Merkel S, Miyagi L, Wenk H R, Shen G, Cynn H and Evans W J 2009 *Rev. Sci. Instrum.* **80** 104501
79. Chen B, Lutker K, Raju S V, Yan J, Kanitpanyacharoen J, Lei J, Yang S, Wenk H R, Mao H K and Williams Q 2012 *Science* **338** 1448-1451
80. Kaercher P, Speziale S, Miyagi L, Kanitpanyacharoen W, and Wenk H R 2012 *Phys. Chem. Minerals* **39** 613-626
81. Wenk H R, Lutterotti L, Kaercher P, Kanitpanyacharoen W, Miyagi L, and Vasin R 2014 *Powder Diffr.* **29** 220-232
82. Yue B B, Hong F, Merkel S, Tan D Y, Yan J Y, Chen B and Mao H K 2016 *Phys. Rev. Lett.* **117** 135701
83. Levitas V I and Preston D L 2002 *Phys. Rev. B* **66** 134207
84. Levitas V I, Chen H and Xiong L 2017 *Phys. Rev. Let.* **118** 025701
85. Levitas V I, Chen H and Xiong L 2017 *Physical Review B* **96** 054118
86. Levitas V I 2013 *Int. J. Plast.* **49** 85-118
87. Feng B and Levitas V I 2017 *International Journal of Plasticity* **96** 156-181
88. Feng B and Levitas V I 2017 *Materials Science and Engineering A.* **680** 130-140
89. Goettel K A, Mao H K and Bell P M 1985 *Rev. Sci. Instrum.* **56** 1420
90. Hemley R J, Mao H K, Shen G, Badro J, Gillet P, Hanfland M, and Häusermann D 1997 *Science* **276** 1242-1245
91. Jeanloz R, Godwal B K and Meade C 1991 *Nature* **349** 687
92. Meade C and Jeanloz R 1988 *Science* **241** 1072
93. Sung C, Goetze C and Mao H K 1977 *Rev. Sci. Instrum.* **48** 1386
94. Vohra Y K, Duclos S J, Brister K E and Ruoff A L 1988 *Phys. Rev. Lett.* **61**
95. Weir S T, Akella J, Ruddle C, Goodwin T and Hsiung L 1998 *Phys. Rev. B* **58**
96. Chen J H, Li L, Weidner D J and Vaughan M T 2004 *Phys. Earth Planet. Inter.* **143** 347-356
97. Duffy T S, Shen G, Heinz D L, Shu J, Ma Y, Hemley R J and Mao H K 1999 *Phys. Rev. B* **60** 15063-15073
98. Hemley R J, Mao H K and Struzhkin V V 2005 *J. Synch. Radiation* **12** 135-154
99. Li L, Weidner D J, Chen J, Vaughan M T, Davis M, and Durham W B 2004 *J. Appl. Phys.* **95** 8357
100. Singh A K 1993 *J. Appl. Phys.* **73** 4278-4286
101. Singh A K and Balasingh C 1994 *J. Appl. Phys.* **75** 4956-4962
102. Singh A K, Hu J, Shu J, Mao H K and Hemley R J 2012 *J. Phys.: Conf. Series* **377** 012008
103. Singh A K, Mao H K, Shu J and Hemley R J 1998 *Phys. Rev. Lett.* **80** 2157-2160
104. Weidner D J 1998 *Ultrahigh-Pressure Mineralogy: Physics and Chemistry of the Earth's Deep Interior. Reviews in Mineralogy* vol 37, ed R J Hemley (Washington, DC: Mineralogical Society of America) pp 493–524
105. Zhao Y and Zhang J 2007 *Appl. Phys. Lett.* **91** 201907
106. *Wang J*, Yang W, *Wang* S, Xiao X, De Carlo F, Liu Y, Mao W L 2012 *J. Appl. Phys.* **111** 112626
107. Zeng Q, Kono Yo, Lin Yu, Zeng Z, Wang J, Sinogeikin S V, Park C, Meng Y, Yang W, Mao H K, and Mao W L 2014 *Phys. Rev. Lett.* **112** 185502

108. Zeng Q S, Lin Y, Liu Y J, Zeng Z D, Shi C Y, Zhang B, Lou H B, Sinogeikin S V, Kono Y, Kenney-Benson C, Park C, Yang W E, Wang W H, Sheng H W, Mao H K, and Mao W L 2016 *Proc. Natl. Acad. Sci. of the USA* **113** 1714-1718
109. Blank V D and Buga S G 1993 *Instruments and Experimental Techniques* **36** 149
110. Buga S G and Blank V D 1993 *High Pressure Physics and Engineering* **3** 40-46
111. Novikov N V, Shvedov L K, Krivosheya Yu N, and Levitas V I 2015 *J of Superhard Materials* **37** 1-7
112. Nomura R. and Uesugi K 2016 *Rev. Sci. Instrum.* **87** 046105
113. Nomura R. Uesugi K Azuma S, Uesugi K, Nakashima Y, Irifune T, Shinmei T, Kakizawa S, Kojima Y, and Kadobayashi H 12017 *Rev. Sci. Instrum.* **88** 044501
114. Merkel S, Hemley R J and Mao H K 1999 *Appl. Phys. Lett.* **74** 656-658
115. Feng B, Levitas V I, Hemley R J 2016 *Int. J. Plast.* **84** 33-57
116. Eisenlohr P, Diehl M and Lebensohn R A et al. 2013 *Int. J. Plasticity* **46** 37-53